LIMNOLOGY and OCEANOGRAPHY

ASLO

Limnol. Oceanogr. 65, 2020, 157–172

doi: 10.1002/lno.11258

Biological modification of seawater chemistry by an ecosystem engineer, the California mussel, *Mytilus californianus*

Aaron Ninokawa,[1]* **Yuichiro Takeshita**,[2] **Brittany M. Jellison**,[1] **Laura J. Jurgens**,[3] **Brian Gaylord**[1,4]

[1]Bodega Marine Laboratory, Bodega Bay, California
[2]Monterey Bay Aquarium Research Institute, Moss Landing, California
[3]Department of Marine Biology, Texas A&M University at Galveston, Galveston, Texas
[4]Department of Evolution and Ecology, University of California, Davis, California

Abstract

Marine habitat-forming species often play critical roles on rocky shores by ameliorating stressful conditions for associated organisms. Such ecosystem engineers provide structure and shelter, for example, by creating refuges from thermal and desiccation stresses at low tide. Less explored is the potential for habitat formers to alter interstitial seawater chemistry during their submergence. Here, we quantify the capacity for dense assemblages of the California mussel, *Mytilus californianus*, to change seawater chemistry (dissolved O_2, pH, and total alkalinity) within the interiors of mussel beds at high tide via respiration and calcification. We established a living mussel bed within a laboratory flow tank and measured vertical pH and oxygen gradients within and above the mussel bed over a range of water velocities. We documented decreases of up to 0.1 pH and 25 μmol O_2 kg^{-1} internal to the bed, along with declines of 100 μmol kg^{-1} in alkalinity, when external flows were < 0.05 m s^{-1}. Although California mussels often live in habitats subjected to much faster velocities, sizeable populations also inhabit bays and estuaries where such moderate flow speeds can occur > 95% of the time. Reductions in pH and O_2 inside mussel beds may negatively impact resident organisms and exacerbate parallel human-induced perturbations to ocean chemistry while potentially selecting for improved tolerance to altered chemistry conditions.

Ecosystem engineers are organisms that create or modify existing habitat in ways that change the properties of the physical environment (Jones et al. 1994). In a number of marine examples (e.g., mussel beds, coral reefs, and kelp forests), such changes occur in association with dense aggregations of individuals that together form biogenic habitats. By providing temporary or permanent homes for many other species (Dayton 1972; Small et al. 1998; Lafferty and Suchanek 2016), ecosystem engineers therefore operate as ecological facilitators for resident taxa, promoting their success (Bruno et al. 2003). They are especially noted for their tendency to ameliorate harsh abiotic stressors like temperature extremes, evaporative water losses, or wave forces, as well as biotic stressors like competition or predation (Bruno et al. 2003; Bulleri 2009). In particular, on rocky shores, low rates of momentum, heat, and mass exchange into and out of aggregations of mussels and macroalgae buffer thermal and desiccation stresses at low tide for organisms living among those aggregations (Jurgens and Gaylord 2018).

However, at high tide or in subtidal locations that are always submerged, such reduced rates of exchange may lead to appreciably altered seawater chemistry within biogenic habitats. These effects have the potential to induce additional performance and/or fitness consequences for organisms on rocky shores. In particular, the reductions in exchange may not only hamper replenishment of food and nutrients, but may also impede the removal of metabolic byproducts. By this mechanism, the biological processes of respiration, photosynthesis, and calcification—due to either the dominant habitat formers or their associated taxa—may drive notable differences between the interstitial seawater and the bulk seawater outside the engineered habitat (Hurd 2015). We can therefore envision that environmental factors promoting respiration, photosynthesis, or calcification should strengthen chemical gradients. By contrast, flow-induced mixing should serve to homogenize conditions inside and outside a dense aggregation, lessening the differences in chemistry. In this regard, the chemical conditions within these habitats will be defined by the balance between physical and biological processes.

Recent work has begun to explore the magnitude and frequency of localized shifts in seawater chemistry within dense assemblages of organisms. Studies to date have focused on those generated by autotrophic organisms where photosynthesis is a dominant process, such as in macroalgal (e.g., Frieder et al. 2012; Cornwall et al. 2013; Hurd 2015; Koweek et al.

*Correspondence: atninokawa@ucdavis.edu

2017; Wahl et al. 2017) and seagrass canopies (e.g., Hendriks et al. 2014; Koweek et al. 2018) and many coral reefs (e.g., Shashar et al. 1993; Agostini et al. 2013). However, less attention has been paid to other habitat formers, such as mussel beds, where respiration and calcification are the key processes perturbing water chemistry (Gutiérrez et al. 2003).

This data gap is important in itself, but has additional relevance to understanding the consequences of human-induced ocean acidification (Caldeira and Wickett 2005). Both respiration and calcification act to increase CO_2 and thus decrease pH and carbonate ion (CO_3^{-2}) concentrations, thereby exacerbating the phenomenon of seawater acidification. Shifts in pH and CO_3^{2-} can be stressful to marine invertebrates that produce a calcium carbonate shell or skeleton (Kroeker et al. 2010; Gazeau et al. 2013), and have potential to induce broader ecological change (Gaylord et al. 2015). For instance, decreases in seawater pH are known to alter species interactions by impairing behavioral responses to key stimuli (Dixson et al. 2010; Munday et al. 2010; Jellison et al. 2016). Oxygen is similarly tied to organismal performance, and is consumed by aggregations of respiring organisms. Numerous studies have documented both lethal and sublethal effects of reduced oxygen concentration (Vaquer-Sunyer and Duarte 2008; Levin et al. 2009). Accordingly, metabolic activities of nonphotosynthesizing habitat-forming species can alter both carbonate chemistry and oxygen concentrations in ways that can negatively impact resident organisms.

On the west coast of North America, extensive aggregations of mussels in the genus *Mytilus* form beds whose interiors experience reduced water exchange (Carrington et al. 2008) and are occupied by an extremely diverse suite of resident species (Kanter 1979; Lafferty and Suchanek 2016). These beds also serve as key recruitment substrate for larvae and juveniles of numerous organisms (Hadfield and Paul 2001; Jurgens and Gaylord 2016), many of which are susceptible to increased CO_2 (Gazeau et al. 2010; Gaylord et al. 2011; Byrne and Przeslawski 2013).

Although there is general consensus that mussels, and bivalves in general, have the ability to alter the chemical properties of seawater in their immediate vicinity (Nixon et al. 1971; Dankers et al. 1989; Asmus et al. 1992; Dame et al. 1992; Khripounoff et al. 2017; Ruginis et al. 2017), the beds themselves are often considered a "black box" and only the chemical fluxes from that box are quantified and reported. As a consequence, relatively little is known about the conditions that actually exist within the interstices of a bed where sensitive organisms live. It is nonetheless these interior seawater conditions that resident organisms experience, rather than the seawater well above the bed where previous studies have tended to take measurements. Based on this observation, we explore, using laboratory flow tank experiments, how seawater chemistry is altered within beds formed by the California mussel, *Mytilus californianus*, an intertidal and subtidal heterotrophic ecosystem engineer. In particular, we investigate the chemical gradients between the bed interior and the surrounding bulk seawater, paying special attention to the countervailing contributions of mussel metabolism, which should strengthen the gradients, and flow-induced mixing, which should weaken the gradients.

Materials and methods

Laboratory experimental overview

Experiments using a laboratory flow tank containing a living mussel bed were conducted in January and February of 2017. During each experiment, seawater pH, O_2, temperature, and salinity were monitored continuously near the top of the tank to quantify bulk water conditions. Additionally, profiles of pH and O_2 above and within the mussel bed were measured to characterize the effects mussel beds have on chemical gradients through their midst. The experiments were conducted at five flow rates (n = 4–6 at each rate). We note that although it is possible in principle to conduct analogous experiments in the field, it is difficult to engage sensitive instrumentation into deeper interstices of mussel beds where the most important deviations in chemistry accrue; in this regard, the present study provides unique insight into conditions that may also be important in the field.

Laboratory mussel bed

Mussels were collected from docks at Spud Point Marina in Bodega Bay, California, in January 2017. Shell characteristics indicated that 90% of the mussels were *M. californianus*. Previous genetic work in the area suggests that the remaining 10% of mussels were likely *Mytilus galloprovincialis* with some *Mytilus trossulus* possible (Saarman and Pogson 2015). Attached epifauna, such as tunicates, were removed immediately following collection. The cleaned mussels were then placed into a recirculating unidirectional flow tank (Engineering Laboratory Design, Model 504), within its working section (45 cm wide by 45 cm high by 2.5 m long). To mimic the attachment of mussels to uneven substrate characteristic of field conditions, an insert of corrugated plastic was used as substrate for the mussels throughout the duration of experiments; this insert also prevented the generation of an along-axis jet of water beneath the mussel bed that might otherwise have tended to form along the bottom wall of the flow tank. The mussels repositioned themselves within the working section, establishing a bed that extended from the leading edge of the working section to 1.8 m downstream, giving a total bed area of 0.81 m^2. Vertically oriented mesh spacers were included transiently in two locations in the bed (Fig. 1) in order to accommodate sensors and were removed during measurements. The mussels were fed 150 mL of Shellfish diet every 1–3 d, after which the water in the flow tank was replaced. Air stones ensured adequate oxygenation between experiments.

Lengths of mussel individuals in the laboratory bed ranged from 0.78 to 23.2 cm with a median of 9.0 cm. Mussel orientations were such that the bed height was approximately 8 cm

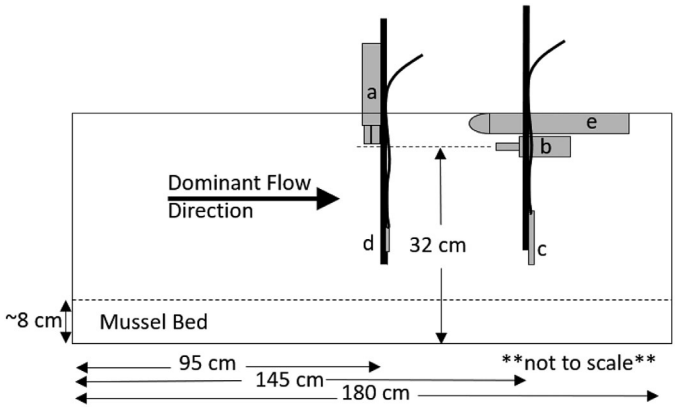

Fig. 1. Schematic of the working section of the flow tank with chemical sensors. The oxygen sensors (letters a and d), and pH sensors (letters b and c) measured chemistry at 4 cm increments vertically while the acoustic Doppler profiler (letter e) measured in 1 cm vertical flow bins throughout the water column. Oxygen and pH profiles were determined at two different horizontal positions in the bed (95 and 145 cm downstream of the leading edge) and sensors were swapped between these two positions.

deep, similar to many beds in the field. At the conclusion of the study, the biomass density of the bed was determined by dissecting 100 mussels, then characterizing the relationship between shell morphology and dry biomass weight (DW) of the tissue in grams. The shell volume in cm^3 (VOL) was approximated using the equation for an ellipsoid, or $VOL = \frac{4}{3}\pi * l * w * h$, where l = along-shell length, w = across-shell width at the apex, and h = the distance across both valves at the apex. For this subset of mussels, a simple linear regression indicated that DW = 0.0035*VOL + 0.2262 (n = 100, r^2 = 0.85). Note that this latter expression is not dimensionally consistent and therefore relies on using the units specified above. Applying this relationship to the entire laboratory bed gave a biomass density of 1.64 $kg\,m^{-2}$, which is similar to other observations of mussel beds in the field (Nixon et al. 1971; Dankers et al. 1989; Asmus et al. 1992).

Experimental setup

Bulk seawater sensors

Oxygen and pH in the bulk seawater were measured at 1 Hz using a Honeywell Durafet III combination electrode (Martz et al. 2010) and a YSI 6920 Sonde with optical DO probe positioned approximately 5 cm below the surface of the tank, or 32 cm above the base of the mussel bed (letters "a" and "b" in Fig. 1). Changes to water chemistry induced by the mussel bed were calculated as deviations from the bulk water measurement. The pH sensor was calibrated on the total scale with bottle samples that were spectrophotometrically analyzed using m-cresol purple (Clayton and Byrne 1993) according to best practices (Martz et al. 2010; Bresnahan et al. 2014). The YSI 6920 Sonde was also fitted with a conductivity/temperature probe to collect temperature and salinity of the water within the flow tank during the experiments. The YSI O_2 measurements were calibrated with measurements from a profiling oxygen sensor, described below.

Profiling sensors

Gradients of pH and O_2 within the mussel bed and in the turbulent boundary layer established over its surface were measured by incrementally raising or lowering sensors to predefined heights above and within the mussel bed. The pH was quantified with a Honeywell Durafet probe using a custom assembly with real-time display (letter "c" in Fig. 1) that recorded once every 3 s, and O_2 was measured using a PreSens Oxygen Microx4 needle-type oxygen microsensor (letter "d" in Fig. 1), recording once per second. Sensors were attached to a 6.4 mm diameter metal rod suspended by a wooden block, allowing the sensors to be raised and lowered through the mussel bed for positioning at precise heights above the bottom. The vertical profiles were collected at two locations in the bed, one near its center and another further downstream (Fig. 1). The pH from the custom Durafet assembly was calibrated to the bulk-sensing Durafet described above while holding the two instruments immediately adjacent. The factory calibration of the profiling O_2 sensor was verified in air-bubbled seawater, assuming 100% saturation. Sensor probes that did not register near 100% saturation were replaced.

Characterization of flow conditions

A Nortek HR 2 MHz Acoustic Doppler Profiler (ADP; Fig. 1) was suspended between the two bed locations, where it measured vertical profiles of horizontal velocity at 1 cm resolution. Horizontal velocities during the experiments followed the "law of the wall" (Boudreau and Jorgensen 2001), whereby:

$$U(z) = \frac{u_*}{\kappa} \ln\left(\frac{z-d}{z_0}\right) \quad (1)$$

where $U(z)$ is the streamwise velocity at height z, u_* is the friction velocity (a measure of wall shear stress), κ is the von Karman constant of 0.41, d is an offset parameter related to the vertical thickness of the mussel bed, and z_0 is the roughness length (Denny 1988; *see* also Gaylord et al. 2006; Stocking et al. 2016). A nonlinear least squares approach was used to fit the law of the wall equation to the velocity profile data, resulting in optimized values for u_*, d, and z_0. Flow conditions, and thus the relative importance of physical mixing, were indexed by the freestream seawater velocity at 32 cm above the base of the bed U_∞. The drag coefficient of the bed was parameterized as $C_d = \frac{u_*^2}{U_\infty^2}$, an index often used to characterize the effect of a surface's physical roughness on flow. Because the suspended particles required by the ADP for reliable sensing quickly settled out of suspension and/or were filtered by the mussels, a mathematical relationship was derived to connect pumping rates of the flow tank to associated flow conditions (U_∞ and u_*). This relationship was determined from periods when the ADP had adequate signal strength to

accurately quantify velocities; these periods were those following water changes when new particles were introduced into the system, and during other times when high flows flushed pseudofeces and sediment from the bed.

Laboratory mussel bed experiments

Flow tank experiments focused on quantifying vertical chemical profiles of oxygen and pH at multiple locations above and within the established mussel bed. Sensors were added to the flow tank within the mussel bed (profiling sensors) and above it (bulk seawater sensors) and were held stationary for 30 min to allow the flow to stabilize and the chemical fluxes to approach steady state. Next, profiling sensors were raised through the water column and held at each height for 2 min to allow the sensors to stabilize. These sensors were raised approximately 4 cm per step until they reached the bulk sensor after which the profiling sensors were lowered through the same heights and intervals again until reaching the bottom. Because the bulk water chemistry was also changing slightly during these procedures due to effects of mussel respiration and calcification on the overall chemistry of the volume of water in the flow tank, profiles of pH and O_2 were expressed relative to the background bulk water values:

$$\Delta C(z) = C(z) - C_\infty \tag{2}$$

yielding the difference in concentrations between the profiling sensor at height z, $C(z)$, and the stationary sensor measuring the bulk water C_∞, at the top of the profile (32 cm above the bottom of the bed). Note that in the above expression, the concentration values apply to either pH or O_2. Because both profiling sensors for pH and O_2 did not fit simultaneously in the bed interstices, profiles for pH and O_2 at a single position were quantified sequentially.

Experiments were conducted across a range of freestream flow speeds, approximately at 0, 0.04, 0.08, 0.17, and 0.27 m s^{-1} (n = 4–6 at each flow rate). Chemical profile data were collected at two different positions within the bed (95 and 145 cm downstream from the start of the leading edge of the bed) to investigate whether downstream position resulted in a different estimate of interstitial chemistry. These efforts resulted in a total of 23 pH profiles and 17 O_2 profiles over a 17-d period. Because background seawater conditions varied across this timespan, experiments also encompassed a range of bulk seawater pH, temperature, and salinity (Table 1).

Calculation of alkalinity gradients and other carbonate parameters

For profiles where both pH and O_2 were available (n = 17), total alkalinity (TA) profiles were estimated by assuming that changes in dissolved inorganic carbon (DIC), resulted from a combination of net community production (the difference between the removal and addition of aqueous CO_2 via photosynthesis or respiration), and net community calcification (NCC, the difference between the removal and addition of DIC via shell precipitation or dissolution). Given a reference alkalinity and changes in O_2 and pH, the change in TA can be estimated by:

$$\Delta \mathrm{TA}(z) = \frac{\Delta O_2(z) \times Q + [\mathrm{DC}(z) - \mathrm{DC}_\infty]\mathrm{TA}_\infty - \mathrm{DC}(z)[\mathrm{B}(z) + \mathrm{OH}(z)] + \mathrm{DC}_\infty[\mathrm{B}_\infty + \mathrm{OH}_\infty]}{\mathrm{DC}(z) - 0.5} \tag{3}$$

where Q is a physiological parameter called the respiratory quotient (ΔDIC/ΔO_2) which does not depend on height z, and TA_∞ is the TA of the bulk water measured at 32 cm (Barnes 1983). The quantity B(z) is the boron concentration derived from salinity, invariant with height in our experiment (Uppstrom 1974) and OH(z) is the hydroxide ion concentration determined from pH at height z. The parameters B_∞ and OH_∞ are the analogous quantities measured at z = 32 cm. The term DC(z) describes the ratio between DIC(z) and carbonate alkalinity (CA(z), *see* Zeebe and Wolf-Gladrow 2001) at height z (or DC_∞ for the bulk water):

$$\mathrm{DC}(z) = \frac{\mathrm{DIC}(z)}{\mathrm{CA}(z)} = \frac{\mathrm{H}(z)k_1 + k_1k_2 + \mathrm{H}(z)^2}{\mathrm{H}(z)k_1 + 2k_1k_2} \tag{4}$$

where $H(z)$ is the hydrogen ion concentration at height z, and k_1 and k_2 are the first and second dissociation constants for carbonic acid (Lueker et al. 2000).

Previous studies utilizing Eqs. 3 and 4 in coral reef systems have assumed Q = 1 (Takeshita et al. 2016, 2018; *see* also Kinsey 1985). For *M. californianus*, Q is also close to 1 (Whedon and Sommer 1937), so a value of 1 was retained here. The calculated TA gradient for the mussel system is relatively insensitive to this choice, as a change of 0.1 in Q only results in a 5% difference of the estimated TA gradient. The respiratory quotient can differ appreciably from 1 in other systems, however, depending on environmental conditions and metabolic substrate (Robinson 2019).

The calculated TA and the pH sensor data were used to determine other parameters of the carbonate system, including dissolved inorganic carbon DIC(z), bicarbonate ion concentration $HCO_3^-(z)$, carbonate ion concentration $CO_3^{-2}(z)$, carbon dioxide concentration $CO_2(z)$, and the calcium

Table 1. Bulk seawater properties during laboratory trials. Bed location 1 indicates measurements were made 95 cm downstream from the lead edge of the bed while bed location 2 refers to measurements at 145 cm downstream.

Profile	Date	Flow velocity*	Bed location	Temperature†	Salinity‡	pH§	O_2‖	HCO_3^{-1}‖	Ω_{Ca}	CO_2¶
1	27 Jan 17	0.15	2	11.25	30.77	7.741	#	1948.7	1.52	816.3
2	27 Jan 17	0.30	2	11.36	30.77	7.692	#	1969.0	1.38	922.8
3	27 Jan 17	0.08	2	11.45	30.77	7.657	#	1983.8	1.29	1008.9
4	29 Jan 17	0.30	2	11.06	30.28	7.815	#	1916.8	1.74	678.0
5	29 Jan 17	0.15	2	11.19	30.28	7.772	#	1932.1	1.60	754.8
6	29 Jan 17	0.08	2	11.26	30.28	7.749	#	1940.0	1.53	799.5
7	2 Feb 17	0.15	2	11.41	29.63	7.781	244.0	1907.1	1.61	732.8
8	2 Feb 17	0.15	1	11.47	29.63	7.763	249.2	1913.1	1.55	767.4
9	3 Feb 17	0.04	2	13.38	29.88	7.729	221.2	1930.6	1.57	847.5
10	3 Feb 17	0.04	1	13.13	29.89	7.699	231.8	1941.3	1.46	912.4
11	7 Feb 17	0.18	1	15.21	28.43	7.754	238.9	1858.8	1.67	787.2
12	7 Feb 17	0.18	2	14.68	28.43	7.724	247.5	1869.3	1.54	843.8
13	7 Feb 17	0.00	2	14.75	28.43	7.597	202.4	1903.5	1.17	1152.2
14	7 Feb 17	0.00	1	14.45	28.43	7.579	202.4	1907.0	1.11	1200.2
15	9 Feb 17	0.04	1	16.56	27.16	7.625	237.4	1854.4	1.27	1075.4
16	9 Feb 17	0.04	2	16.05	27.16	7.607	243.6	1864.8	1.20	1123.0
17	11 Feb 17	0.00	1	12.51	30.19	7.760	217.9	1799.2	1.53	729.7
18	11 Feb 17	0.00	2	12.59	30.19	7.708	238.0	1818.6	1.37	832.7
19	13 Feb 17	0.09	1	15.34	30.22	7.591	233.2	1915.7	1.23	1169.4
20	13 Feb 17	0.18	1	14.87	30.22	7.577	229.5	1921.5	1.17	1208.7
21	13 Feb 17	0.18	2	15.24	30.22	7.535	229.8	1930.3	1.09	1338.8
22	13 Feb 17	0.24	1	15.02	30.22	7.561	229.5	1924.8	1.14	1255.6
23	13 Feb 17	0.24	2	15.12	30.22	7.545	229.8	1928.3	1.11	1305.7

*Units are m s^{-1}.
†Units are°C.
‡Units are PSU.
§pH is on the total scale.
‖Units are μmol kg^{-1}.
¶Units are μatm.
#No oxygen data.

carbonate saturation state for calcite $\Omega_{Ca}(z)$. Saturation state is the product of calcium and carbonate concentrations divided by the solubility constant for calcite, and describes the thermodynamic tendency of calcium carbonate to form or dissolve, where values less than 1.0 indicate a propensity for dissolution (Zeebe and Wolf-Gladrow 2001; although also *see* Ries et al. 2016). Carbonate system analyses were carried out using the package seacarb (Gattuso et al. 2018) in the statistical software *R*, using equilibrium constants from Lueker et al. (2000).

Mussel respiration and calcification rates

The respiration (R) and calcification (NCC) rates of the mussels, calculated per surface area of the bed, were quantified using the gradient flux approach. This method approximates chemical fluxes as diffusive processes and assumes that mass and momentum adhere to identical patterns of turbulence-induced mixing across the boundary layer (Bird et al. 1960; McGillis et al. 2011; Takeshita et al. 2016).

Following Takeshita et al. (2016), a chemical's concentration at a given height z, $C(z)$, above a surface and for a given flow speed can be expressed as:

$$C(z) = -\frac{J}{u_* \kappa} \ln\left(\frac{z}{z_{0,c}}\right) \quad (5)$$

where $z_{0,c}$ is a scaling parameter similar to roughness length and J is the flux of the constituent described by Fick's first law of diffusion, $J = -K_z \frac{\partial C}{\partial z}$, where K_z is the eddy diffusivity, a measure of the rate of vertical turbulent mixing, and positive J indicates fluxes out of the bed. In a turbulent boundary layer, $K_z = \kappa u_* z$. To generate an expression that has the same interpretation as the ΔO_2 and ΔTA profiles, $C(z)$ can be subtracted from C_∞:

$$\Delta C(z) = \frac{J}{u_* \kappa} \ln\left(\frac{z}{z_\infty}\right) \quad (6)$$

This expression has the further advantage of eliminating the $z_{o,c}$ scaling parameter. It is possible to solve Eq. 6 for the

fluxes (J) for each of oxygen and alkalinity, and assuming steady state, and then to estimate respiration (R) and calcification (NCC) rates as:

$$R = -J_{O_2} \quad (7)$$

$$\mathrm{NCC} = -0.5\, J_{\mathrm{TA}} \quad (8)$$

where the subscripts indicate the chemical parameter of interest. The −0.5 coefficient for NCC arises from the stoichiometric ratio of alkalinity flux to calcium carbonate formed (Zeebe and Wolf-Gladrow 2001). Note that the assumption of a turbulent boundary layer prevents the use of this calculation methodology when flows are negligible. Thus, rates were not calculated under conditions of zero flow (n = 4) for this study.

A second estimate of respiration rate R_∞ was also calculated from changes through time in bulk water oxygen $O_{2,\infty}$ assuming minimal gas exchange across the free surface of the water and a well-mixed tank. With these assumptions, the system can be modeled as closed, meaning that changes in $O_{2,\infty}$ should be driven solely by respiration. Assuming that the benthic respiration due to the mussels dominates over any respiration occurring in the water column (e.g., due to microorganisms in the water), R_∞ can be expressed as:

$$R_\infty = \frac{\Delta O_{2,\infty}}{\Delta \mathrm{time}} \times \frac{\mathrm{volume}}{\mathrm{area}} \quad (9)$$

where the volume of the tank was 4.715 m^3 and the area of the mussel bed was 0.81 m^2. This second approach provides an opportunity to compare rates calculated based on Eqs. 5–8. Oxygen fluxes across the surface of the flow tank were minimal (0.46 ± 0.41 mmol O_2 m^{-2} h^{-1}, mean ± SD) and were not included in calculations of benthic oxygen flux. Air–water oxygen fluxes were calculated by multiplying the oxygen gradient by gas transfer velocity coefficient available in the R package, marelac (Soetaert et al. 2018).

Statistical relationships for in-bed chemistry

The maximum observed chemical differences between the bulk water and seawater in the interior of the mussel bed $\Delta C_{\max}$ were examined for each profile. This maximum difference was quantified at the lowest measurement height within the mussel bed (z = 0). Statistical model selection using a multiple linear regression framework was performed by starting with velocity, R, NCC, and all interactions and incrementally dropping nonsignificant terms following Burnham and Anderson (2002). This initial evaluation revealed a dependence of $\Delta C_{\max}$ on both velocity and R or NCC, of the form

$$\log(-\Delta C_{\max}) = a_0 + a_1 U_\infty + a_2 R + a_3 \mathrm{NCC} \quad (10)$$

where a_0, a_1, a_2, and a_3 are the regression coefficients and $\Delta C_{\max}$ was log transformed to meet assumptions of normality while also ensuring that the model appropriately allowed $\Delta C_{\max}$ to approach zero but not cross it as velocity increased.

Flow velocities in the field

In order to contextualize the water velocities measured in the laboratory, an acoustic Doppler velocimeter (ADV; Nortek Vector) was deployed from 11 July 2017 to 24 July 2017, and recorded three-dimensional water velocities at a frequency of 1 Hz over multiple tidal cycles in the field near the mussel collection site. Horizontal water velocities were extracted from the ADV data using the oce package (Kelley and Richards 2018) in the statistical software R. This data set was used to estimate the percentage of time that mussel beds at the collection site experienced freestream seawater velocities below a given magnitude. These estimates were combined in turn with the relationship of Eq. 10, based on mean rates of respiration (R) and calcification (NCC), to bound the percentage of time organisms living within mussel beds at field sites similar to the one we examined might experience certain chemistry conditions. Note that the estimates developed using this approach can be expected to apply only to subtidal mussel beds living in habitats comparable to our field site, and may not hold in other situations or locations. In particular, it would likely be inappropriate to extrapolate these estimates to *M. californianus* beds occurring on wave-exposed rocky coasts, where much faster flows at high tide create conditions that diverge markedly from those explored in the present study.

Measurements of pH in a field mussel bed

A first-order examination of the extent of consistency between the laboratory data and field conditions was conducted by deploying the profiling pH sensor on 21 February 2019 inside a mussel bed growing at the collection site. The fragility of the oxygen sensor prevented its use in the field. The mussel bed at the field site was approximately 10 cm deep. However, in this natural bed, it was not possible to find gaps between mussels (for the insertion of the pH sensor) that reached entirely to the base of the bed. Therefore, the field pH data extended only halfway through the thickness of the aggregation. Freestream pH values outside the bed were then recorded 25 cm above the base of the bed at a frequency of 1 Hz, and the sensor was alternated between above-bed and within-bed locations, allowing 3 min for each reading to stabilize. Measurements were made in three different positions along the length of the field mussel bed. Water velocities were quantified concomitantly with the pH measurements using an ADV (Nortek Vetrino) measuring at 25 Hz also placed 25 cm above the base of the bed.

Results

Bulk seawater chemistry

Bulk seawater chemistry varied between experimental days (Table 1) due to changing hydrographic conditions in waters offshore of Bodega Marine Laboratory where the seawater

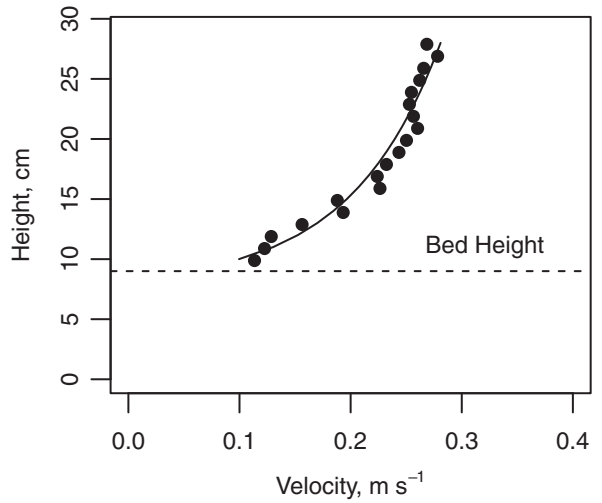

Fig. 2. Representative velocity profile recorded in the laboratory flow tank above the experimental mussel bed. Solid circles indicate the average streamwise velocities at a given height, recorded over a 3-min sampling period. The line is the best fit to Eq. 1 with z_0 = 0.7 cm, d = 7.8 cm, and u_* = 0.034 m s^{-1}. The freestream velocity associated with this profile was 0.30 m s^{-1}.

originated. The bulk seawater pH ranged from 7.535 to 7.815 while bulk seawater O_2 ranged from 203.2 to 249.2 μmol kg^{-1}. Due to mussel metabolism, bulk seawater pH changed by −0.026 pH h^{-1}, on average, while bulk seawater O_2 changed by −8.46 μmol kg^{-1} h^{-1}, on average, in the flow tank during the time it took to measure a profile (approximately 45 min). Chemistry within the bed changed at similar rates so that the concentration difference profiles remained relatively constant through time satisfying assumptions of steady state. Temperature and salinity did not change substantially during a profile, exhibiting average rates of change of 0.24°C h^{-1} and 0.002 PSU h^{-1}, respectively.

Flow profiles

Horizontal velocities above the bed surface in the flow tank generally followed the "law of the wall" given by Eq. 1 (Fig. 2). Freestream velocities U_∞ ranged between 0 and 0.30 m s^{-1}. The friction velocities u_* were 9.4% of the freestream velocities, on average, leading to a drag coefficient C_d of 0.009. The average canopy height d and roughness length parameters z_0 were 8.8 and 0.6 cm, respectively, and showed no correlation with freestream velocity ($r < 0.26$, $p > 0.37$). These values are within the range of others from analogous systems (Green et al. 1998).

Vertical pH and O_2 profiles

Seawater pH and O_2 concentrations were lower in the mussel bed than in the bulk seawater (Fig. 3). The pH and oxygen gradients also steepened as measurements approached the base of the bed. This relationship intensified with decreasing flow speed as there were greater differences between the bulk and in-bed chemistries at lower velocities than at higher ones (Fig. 3 and Table 2). For example, in the absence of flow, the mean differences in pH and O_2 (± standard deviation) between the bulk water and the bottom of the mussel bed (z = 0) were −0.069 (± 0.026) pH and −21.9 (± 8.9) μmol O_2 kg^{-1}, respectively. Maximum observed differences were −0.119 pH at 0.043 m s^{-1} and −40.7 μmol O_2 kg^{-1} at 0 m s^{-1}. Note that the maximum difference in pH was not always observed in the absence of flow which is likely due to differences in the mussel respiration and calcification rates (*see* the Statistical predictors of in-bed chemistry section below). Mean differences in pH and O_2 were −0.033 (± 0.016) pH at 0.27 m s^{-1} and −4.15 (± 3.0) μmol O_2 kg^{-1} at 0.27 m s^{-1}. Minimum observed differences were −0.011 pH at 0.18 m s^{-1} and −0.45 μmol O_2 kg^{-1} at 0.27 m s^{-1}. TA, as calculated from Eq. 3, followed the same pattern and the mean difference between the base of the bed and bulk water was −68.2 (± 31.0) μmol kg^{-1} in the absence of flow, whereas the mean difference was −18.3 (± 4.3) μmol kg^{-1} at a flow speed of 0.27 m s^{-1}. The mean saturation state of calcite at the base of the bed was lower than that of the bulk water by up to 0.28 (± 0.10) units at a flow speed of 0.04 m s^{-1}, dropping to a difference in Ω_{Ca} of 0.10 (± 0.06) at 0.17 m s^{-1}.

Mussel respiration and calcification

Respiration (R) and calcification (NCC) calculated from the oxygen and alkalinity fluxes ranged from 0.52 to 59.1 mmol O_2 m^{-2} h^{-1} and from 29.8 to 186.6 mmol $CaCO_3$ m^{-2} h^{-1}, respectively, under nonzero flow rates (Table 2). The respiration rates calculated via the flux-gradient method (Eqs. 6 and 7) vs. those estimated from the bulk water oxygen change (Eq. 9) were not significantly different (paired t-test, t = 0.71, df = 12, p = 0.49, Fig. 4). There was no significant difference between R, NCC, or maximum inside–outside difference (ΔC_{max}) in pH or oxygen at the two positions downstream of the leading edge of the bed (paired t-tests, $p > 0.35$ in all cases). As such, all subsequent analyses combined data from both positions.

Statistical predictors of in-bed chemistry

The statistical model of Eq. 10 revealed that higher mussel bed respiration and calcification increased observed differences in chemistry between seawater inside and outside the bed. In contrast, faster flow speeds increased turbulent mixing, which decreased the differences (Fig. 5 and Table 3). The maximum difference (ΔC_{max}) between within-bed oxygen and values of oxygen in the bulk waters was best predicted by flow rate and respiration R (Table 3). On the other hand, maximum chemical differences between interior and above-bed pH, TA, and Ω_{Ca} were best predicted by flow rate and calcification NCC (Table 3). No interaction terms were significant. In all cases, increases in mussel biological rates (R and NCC) led to greater differences between the seawater chemistry within the mussel bed and the chemistry above it (Fig. 5).

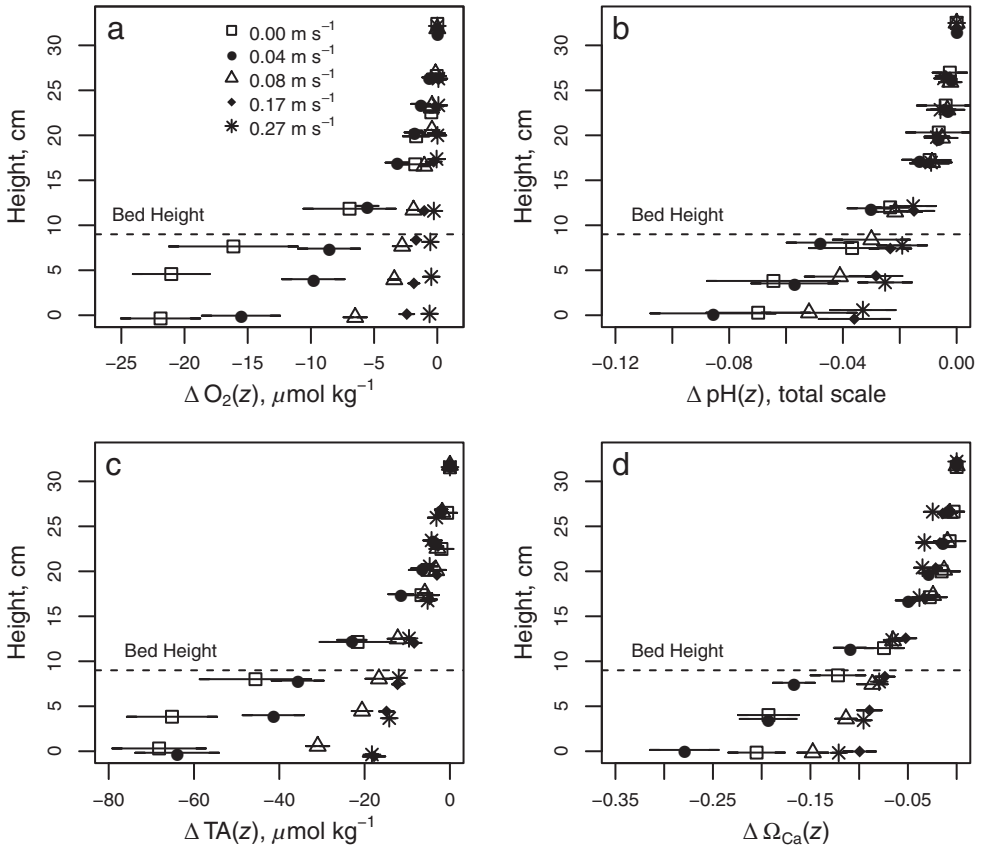

Fig. 3. Seawater chemistry is altered within the mussel bed. Vertical difference profiles for (**a**) oxygen, (**b**) pH, (**c**) total alkalinity (TA), and (**d**) calcite saturation state (Ω_{Ca}) indicate that all of these chemical parameters are lower inside the bed compared to the bulk seawater. Error bars depict the standard error across multiple profiles within each flow bin. Data have been jittered in the *y* axis for visibility.

Field flow velocities

Flow speeds recorded within the estuarine field site of the study ranged between 0 and 0.86 m s^{-1}. Velocity magnitudes were below 0.01 m s^{-1} for 50% of the time and below 0.05 m s^{-1} for 98% of the time (Fig. 6). Applying this distribution of flow rates and inserting a mean respiration rate (30.21 mmol O_2 m^{-2} h^{-1}) and a mean calcification rate (94.4 mmol $CaCO_3$ m^{-2} h^{-1}) into the previously described statistical model (Eq. 10; Table 3) yields an expected frequency that residents within a mussel bed would encounter various levels of chemical perturbation. This approach suggests that organisms living near the bottom of estuarine mussel beds in locations similar to the field collection site of the present study could spend up to 98% of their time in seawater characterized by reductions of 12.1 μmol O_2 kg^{-1}, 0.1 pH, 75.3 μmol alkalinity kg^{-1}, and 0.26 Ω_{Ca} relative to the surrounding bulk seawater.

Field mussel bed pH

The pH of seawater external to the bed at the field collection site was 7.952 units. The pH within three locations in the interstices of the same bed was 7.942, 7.923, and 7.930, respectively. These values indicate decreases in pH of 0.010, 0.029, and 0.022 units, respectively, at locations halfway down to the base of a mussel bed. Mean seawater velocity above the field mussel bed was 0.09 m s^{-1}, directed along the primary axis of the mussel bed. Mean flow velocities along other axes were minimal (< 0.001 m s^{-1}). At this flow velocity and assuming that the field mussel bed exhibited the mean NCC (94.4 mmol $CaCO_3$ m^{-2} h^{-1}) of the laboratory bed, the expected pH decrease was 0.066 units. If considering the full range of NCC rates observed in the laboratory mussel bed (between 29.8 and 186.6 mmol $CaCO_3$ m^{-2} h^{-1}), the expected pH decrease ranged between 0.027 and 0.178 units. Since the pH sensor could not reach the bottom of the field bed, a more appropriate comparison to laboratory data might be the expected pH decrease at 4 cm above the base of the bed. At 4 cm above the base of the bed, the expected range of pH decrease was from 0.020 to 0.126 units.

Discussion

Chemical conditions within a mussel bed

Habitat-forming mussels can clearly alter seawater chemistry within the interstices of the beds they form. As they

Table 2. Chemical fluxes (NCC, calcification; *R*, respiration), within-bed seawater chemistry, and maximum observed difference of each chemical parameter from that of the bulk water, for each profile.

	Fluxes		Within-bed seawater chemistry					Maximum observed differences (ΔC_{max})				
Profile	NCC*	R*	pH	O_2†	HCO_3^{-1}†	Ω_{Ca}	CO_2‡	pH	O_2†	HCO_3^{-1}†	Ω_{Ca}	CO_2‡
1	§	§	7.711	§	§	§	§	−0.029	§	§	§	§
2	§	§	7.674	§	§	§	§	−0.019	§	§	§	§
3	§	§	7.605	§	§	§	§	−0.052	§	§	§	§
4	§	§	7.794	§	§	§	§	−0.021	§	§	§	§
5	§	§	7.721	§	§	§	§	−0.051	§	§	§	§
6	§	§	7.683	§	§	§	§	−0.066	§	§	§	§
7	105.6	75.9	7.742	238.0	1892.7	1.48	796.8	−0.040	−6.0	−14.3	−0.13	64.0
8	62.3	42.2	7.742	240.7	1896.0	1.48	797.3	−0.020	−8.5	−17.1	−0.07	29.9
9	87.8	41.9	7.639	194.7	1873.5	1.29	1012.7	−0.090	−26.6	−57.0	−0.28	165.2
10	109.8	59.1	7.586	214.0	1897.0	1.14	1154.5	−0.112	−17.8	−44.3	−0.31	242.1
11	84.7	44.7	7.743	236.8	1853.8	1.63	804.5	−0.011	−2.1	−5.0	−0.04	17.3
12	49.7	19.4	7.711	244.8	1863.5	1.49	867.2	−0.013	−2.7	−5.8	−0.04	23.4
13	‖	‖	7.516	178.4	1847.3	0.98	1347.6	−0.081	−24.0	−56.3	−0.19	195.4
14	‖	‖	7.486	172.9	1835.5	0.91	1432.0	−0.093	−29.5	−71.5	−0.21	231.7
15	29.8	9.0	7.582	232.4	1841.0	1.16	1178.7	−0.043	−5.0	−13.4	−0.11	103.3
16	58.4	30.8	7.509	230.7	1828.8	0.97	1380.4	−0.098	−12.9	−36.0	−0.23	257.4
17	‖	‖	7.718	204.4	1772.4	1.39	792.3	−0.042	−13.5	−26.8	−0.13	62.5
18	‖	‖	7.654	220.2	1780.7	1.22	922.9	−0.054	−17.8	−37.9	−0.15	90.3
19	115.6	17.9	7.510	228.9	1899.0	1.03	1398.2	−0.081	−4.3	−16.7	−0.20	228.8
20	185.5	13.9	7.512	227.6	1910.4	1.02	1393.0	−0.064	−2.0	−11.0	−0.15	184.3
21	101.6	19.5	7.487	227.2	1918.9	0.98	1489.2	−0.049	−2.6	−11.4	−0.11	150.4
22	186.6	17.9	7.509	228.8	1917.3	1.02	1411.0	−0.052	−0.7	−7.6	−0.12	155.4
23	121.8	0.5	7.506	229.5	1922.6	1.02	1426.0	−0.040	−0.3	−5.7	−0.09	120.3

*Units are mmol h^{-1} m^{-2}.
†Units are μmol kg^{-1}.
‡Units are μatm.
§No oxygen data, preventing calculation of alkalinity profiles and chemical fluxes.
‖Flow rate too slow to induce adequate turbulent mixing.

respire, they decrease O_2 and increase CO_2. Likewise, calcification decreases TA and DIC and increases carbon dioxide. Together, these processes reduce the pH of the seawater in the bed interior (Fig. 3 and Table 2). Such pH declines reach more than 0.1 units below values of the external seawater under flow speeds common in the field. This level of depression corresponds to declines expected in open-ocean waters decades sooner than expected (Caldeira and Wickett 2005). Our data also indicate that mussels can decrease the calcite saturation state within the bed by almost 0.30 relative to bulk water. As with the pH gradients, these differences diminish at higher flow rates due to more vigorous turbulent mixing of external waters into the bed, but remain large enough to potentially influence the performance of organisms that live within the confines of this ecosystem engineer (Ries et al. 2009). This situation holds especially in hydrodynamically benign locales such as bays and estuaries where flow speeds may routinely be 0.05 m s^{-1} or less (Fig. 6). At the field collection site of the present study when external flow speeds were approximately 0.09 m s^{-1}, the pH inside the bed at a height 5 cm above its base was 0.021 units below that outside on average. Our laboratory data would predict a somewhat greater pH difference (~ 0.066; Fig. 3). There are a multitude of possibilities why this may be the case including enhanced mixing, lower NCC in the field than in the laboratory, or even the inability to reach the base of the field mussel bed. Given that the range of predicted pH decreases at 4 cm encompasses some of the field observations, there is some support for the latter explanation. Further experiments are required to evaluate whether the greater hydrodynamic complexity of field conditions might have been responsible for the smaller gradients in pH, or whether methodological considerations might also apply.

Higher mussel respiration and calcification rates strengthen chemical differences between waters in the bed interior vs. those outside (Fig. 5). Given that the biological processes of respiration and calcification drive the major chemical differences between the within-bed and above-bed seawater, environmental factors influencing these rates will indirectly control within-bed chemistry. For example, temperature and salinity are known to influence mussel respiration (Stickle and

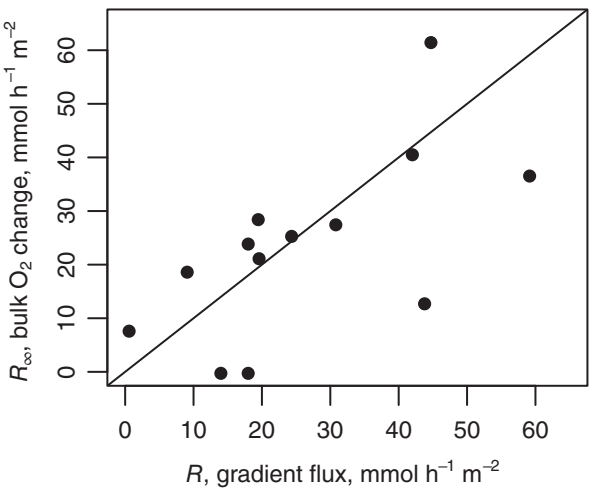

Fig. 4. Respiration estimates computed using the gradient flux method (R, Eqs. 6 and 7) are statistically indistinguishable from those calculated from the deviation in bulk water conditions (R_∞, Eq. 9). The solid line depicts a 1:1 relationship. A small subset (n = 4) of profiles that did not satisfy assumptions of steady state or finite fluid velocity was excluded.

Sabourin 1979; Jansen et al. 2009) and calcification (Malone and Dodd 1967). Here, we observed a correlation between respiration and temperature (r = –0.76, p = 0.003) and between calcification and salinity (r = 0.74, p = 0.004, Fig. 7a), suggesting that these two abiotic parameters do have the potential to indirectly influence seawater chemistry within a mussel bed via the modification of biological rates.

An additional complexity arises when considering that other drivers of respiration and calcification are directly involved with those biological processes either as substrates or as waste products. For example, in the calcification process, bicarbonate ions, HCO_3^-, are consumed and hydronium ions are produced (Thomsen et al. 2015). This recognized linkage has led to interest in understanding whether the ratio of bicarbonate to hydronium concentration, termed the substrate to inhibitor ratio (SIR), might index calcification potential in calcium carbonate-forming organisms (Jokiel 2013; Fassbender et al. 2016). Under certain contexts, SIR values might operate as an alternative to the calcium carbonate saturation state Ω_{Ca} in describing whether seawater is favorable for calcification

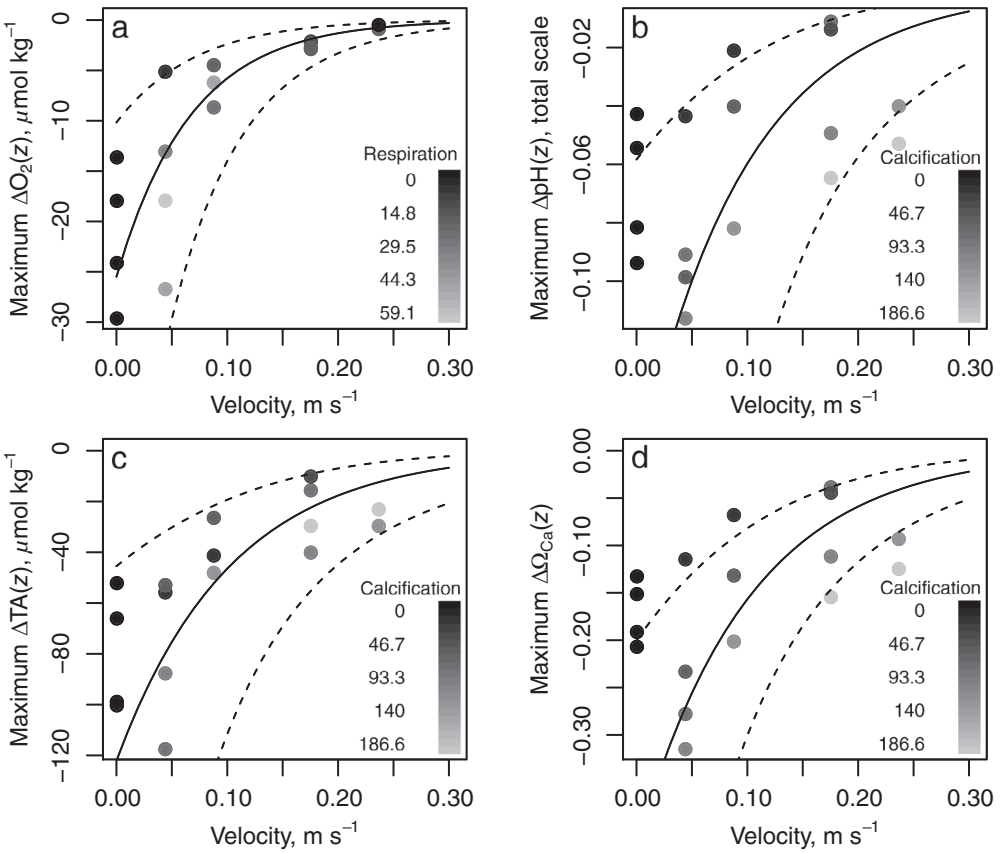

Fig. 5. Seawater chemistry in the mussel bed is driven by flow velocity and mussel respiration R or net community calcification NCC (*see* Table 3 for details). (**a**) Oxygen differences were best predicted by respiration and seawater velocity while (**b**) pH, (**c**) total alkalinity (TA), and (**d**) carbonate saturation state of calcite (Ω_{Ca}) differences were best predicted by calcification and seawater velocity. Points shown correspond to the 0 cm vertical data from the concentration difference profiles. Shading of the points indicates the mussel respiration (R, mmol O_2 m^{-2} h^{-1}) or calcification rate (NCC, mmol $CaCO_3$ m^{-2} h^{-1}) as calculated via Eqs. 6–8. Lines are predictions from the best fitting statistical model (Table 3) assuming mean respiration rate (R) = 30.21 mmol O_2 m^{-2} h^{-1}or mean net community calcification rate (NCC) = 94.4 mmol $CaCO_3$ m^{-2} h^{-1}. Points at zero velocity are shown for completeness but were not included in the model fits and do not have a corresponding respiration or calcification rate. Dashed lines give the prediction intervals from each corresponding model.

Table 3. Results of multiple linear regressions examining the effects of seawater velocity (m s^{-1}), mussel calcification (NCC, μmol h^{-1} m^{-2}), and mussel respiration (R, μmol h^{-1} m^{-2}) on the differences between within and above-bed seawater chemistry. The units of ΔO_2 and ΔAlkalinity are μmol kg^{-1}. Each equation is in the format, $\ln(-\Delta C) \sim a_0 + a_1 U_\infty + a_2 \text{NCC} + a_3 R$.

	Model coefficients (SD)						
Response (ΔC)	**a_0**	**a_1**	**a_2**	**a_3**	**$F_{2,14}$ statistic**	**Model R^2**	**Model p-value**
ΔO_2	2.89 (0.18)	−14.84 (1.20)	—	0.013 (0.005)	77.2	0.92	<0.0001
ΔpH	−2.91 (0.17)	−10.30 (1.94)	0.0112 (0.003)	—	14.2	0.67	0.0004
ΔAlkalinity	4.23 (0.16)	−9.67 (1.82)	0.006 (0.003)	—	17.4	0.71	0.0002
$\Delta\Omega_{Ca}$	−1.88 (0.12)	−9.79 (1.35)	0.011 (0.002)	—	29.29	0.79	<0.0001

(Green et al. 2009; Waldbusser et al. 2015). We did not observe NCC to be sensitive to either SIR or Ω_{Ca} ($p > 0.14$, Fig. 7b), which has been observed in other mussels (Ries et al. 2009) and corals (Comeau et al. 2018). We did, however, observe a correlation between HCO_3^- concentration and calcification ($r = 0.74$, $p = 0.003$, Fig. 7c) hinting that our mussels might be substrate limited (Thomsen et al. 2015). If such is the case, given that HCO_3^- concentrations can be lower inside the bed (Fig. 7d), there could be important implications for resident taxa. Specifically, at high mussel densities and comparatively slow flows, shell-forming taxa interior to a mussel bed may experience substrate limits on calcification. That said, a high correlation between bicarbonate ion concentration and salinity in our experiments ($r = 0.93$) prevents firmer conclusions from being drawn at present.

If there are feedbacks between mussel metabolism and the chemical conditions they create inside their assemblages, then mixing processes become even more important to the success of mussels and the residents of their beds. Because the mixing of oxygen and substrates for calcification into the bed is required for sustained respiration and calcification, it is important to consider the ambient flow environment. This includes how it interacts with bed properties like organism density, geometry, and morphology. Much work to date has focused on the effects of flow on photosynthesizing macroalgae and corals and many of the core principles are the same. In general, higher flow rates increase mixing and allow for higher metabolic rates until mass transfer is no longer limiting (Hurd 2000, 2015; Chan et al. 2016). In mussel beds, we would expect that stronger mixing, such as by increased turbulence via higher seawater velocities, will better homogenize the in-bed and bulk seawater chemistries. Bed roughness and drag could also influence exchange by inducing greater mixing for a given velocity. However, because many natural beds exhibit a lower drag coefficient than that of our bed (Green et al. 1998) and may be fouled by epiphytic algae that can reduce exchange through their canopies (Witman and Suchanek 1984; Stocking et al. 2016), it is likely that chemical differences between the exteriors and interiors of other mussel beds will vary.

There are also other habitat forming bivalves beyond California mussels (Table 4). We would expect that chemical perturbations similar to the ones we observed here would accrue for most of these taxa. However, given the wide range of respiration rates measured for these organisms, along with probable differences in rates of calcification and the spectrum of habitats in which they live, the magnitude of these perturbations would likely vary. Nevertheless, regardless of the exact biological rates, the effect of these bivalves would be to drive pH and O_2 concentrations lower than those of the bulk water. Similarly, we expect that the addition of autotrophic algae to the community would likely buffer mussel effects during the day when photosynthesis removes CO_2 and replenishes O_2. However, it would accentuate acidification and O_2 depletion during the night. Indeed, benthic community metabolism is well known to alter chemical fluxes and seawater chemistry (Lantz et al. 2014; Kwiatkowski et al. 2016; Page et al. 2016). Testing the effects of the full community (not just the mussels) on chemistry interior to an aggregation is

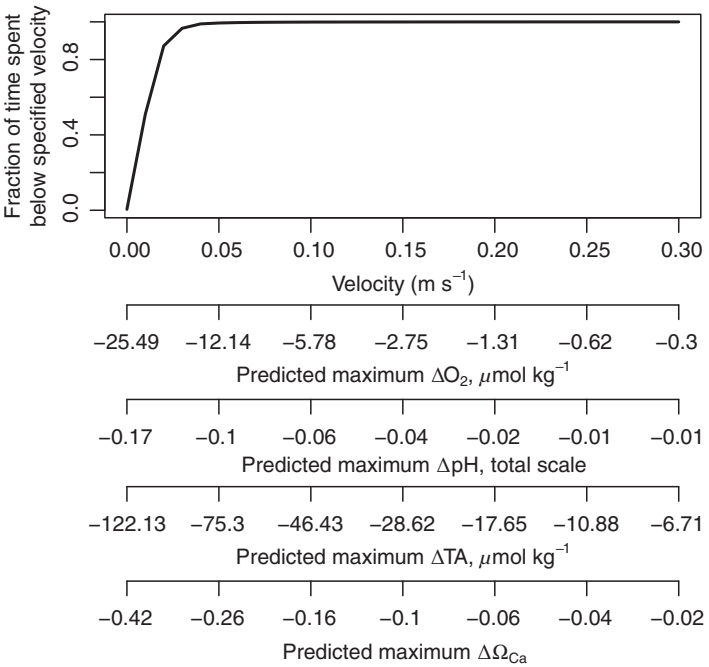

Fig. 6. Observed frequencies of flow speeds less than a given velocity based on field data collected in Bodega Harbor, Bodega Bay, California. Additional x axes show maximal chemical differences between external waters and those at the base of a mussel bed, as predicted from best fitting models for each parameter assuming a value for mean respiration (R) = 30.21 mmol O_2 m^{-2} h^{-1} or mean net community calcification rate (NCC) = 94.4 mmol $CaCO_3$ m^{-2} h^{-1} (*see* Table 3).

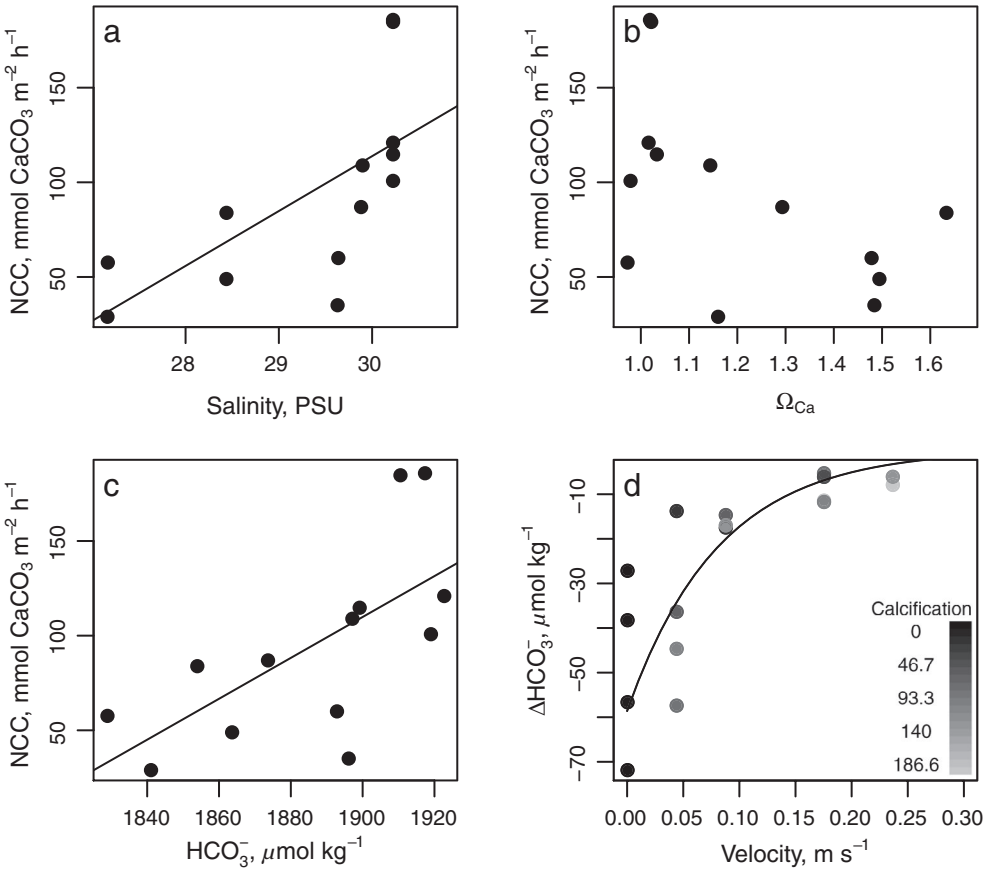

Fig. 7. Exploration of various possible controls on mussel bed net community calcification rates (NCC). (**a**) There was a significant correlation between salinity and NCC. (**b**) There was no correlation between NCC and calcite saturation state, Ω_{Ca}. (**c**, **d**) Relationships between bicarbonate ion (HCO_3^-) and NCC highlight the potential for feedbacks in mussel beds. Calcification appears to be enhanced under higher bicarbonate concentration, but higher calcification rates, especially under slow flow, depress bicarbonate ion concentrations.

Table 4. Examples of other bed-forming bivalve assemblages and their reported respiration rates *R* calculated as oxygen fluxes. Note that, unless otherwise specified, fluxes represent whole communities associated with the bivalve assemblage, either within the bed matrix or in the water or sediment above or below the bed. As such, negative *R* indicates that the community is net photosynthetic.

Species	Location	Biomass density*	Maximum $R^{\dagger}$	Minimum $R^{\dagger}$	Source
Mytilus californianus‡	Bodega Harbor, California (Laboratory)	1.64	59.1	0.6	This study
Mytilus edulis	Narragansett Bay, Rhode Island	1.55	84.4	6.3	Nixon et al. (1971)
Mytilus edulis‡	Texel, Wadden Sea (Laboratory)	1.54	31.2	15.6	Dankers et al. (1989)
Mytilus edulis	Texel, Wadden Sea	0.82	306	−12.5	Dankers et al. (1989)
Mytilus edulis‡	Sylt, Wadden Sea	2.58	278	18.8	Asmus et al. (1992)
Crassostrea virginica	North Inlet, South Carolina	0.20	125	−46.9	Dame et al. (1992)
Dreisena polymorpha‡	Plateliai Lake, Lithuania	0.04–0.13	5.1	1	Ruginis et al. (2017)
Christineconcha regab	Gulf of Guinea, West Africa	1.07–0.16	20.5	1.8	Khripounoff et al. (2017)
Bathmodiolis boomerang	Gulf of Guinea, West Africa	0.08–0.09	1.4	1.3	Khripounoff et al. (2017)
Abyssogena southwardae	Gulf of Guinea, West Africa	0.33	2.0		Khripounoff et al. (2017)
Calyptogena valdiviae	Gulf of Guinea, West Africa		11.3	1.2	Khripounoff et al. (2017)

*Units are kg m^{-2}.
†Units are mmol m^{-2} h^{-1}.
‡Indicates where communities were simplified to just the listed bivalve by physical removal of other species or by correcting for sediment and pelagic fluxes with a control.

a necessary future step to fully understand the chemical environment of natural beds.

Broader implications for bed residents

In considering possible population implications of altered chemical conditions within mussel beds—both currently and into the future—certain life stages of affected taxa may be most sensitive. For example, impaired habitat selection and reduced survival are possible for recruits of diverse taxa that preferentially settle into mussel beds (Hadfield and Paul 2001). Recent settlers are vulnerable to many stresses, including heat, desiccation, and predation, that can drive high mortality and, given their sensitivity to elevated pCO_2 (Kurihara 2008; Byrne 2011), it is plausible that the altered seawater chemistry within mussel beds could contribute to that mortality. Additionally, some species, including mussels, can undergo a secondary settlement phase. Mytilid mussels, for example, typically start their post-larval period attached to filamentous algae or settle within the mussel bed on byssal threads of adults (Bayne 1964) and eventually shift to the mussel bed surface (Jurgens and Gaylord 2016). Seawater chemistry might influence these movements, as different types of habitat (e.g., heterotrophic ones like mussel beds vs. autotrophic habitats like seaweed and seagrass stands), or locations within the habitat (e.g., the mussel bed surface or interior), may create either more suitable or less preferable interstitial chemical environments for early life stages. Although chemistry is likely not the sole factor dictating habitat selection processes, effects of chemical habitat heterogeneity would be worth testing further given our findings here. Even if this heterogeneity is not a significant driver of habitat selection in a modern ocean, it may become more important in the future as oceans change (Jurgens and Gaylord 2018).

In the context of global ocean change, the capacity of this ecosystem engineer to reduce local pH (Figs. 3 and 5) highlights the potential for low-pH projections to be reached sooner than expected in such heterotrophic habitats. The decrease in pH driven by our experimental mussel bed is equivalent, at its maximum, to the amount observed in surface waters of the open ocean due to anthropogenic CO_2 addition since preindustrial times (Caldeira and Wickett 2003). This magnitude of within-bed pH reduction is also nearly 20% of the expected 0.3 pH decrease expected by the year 2100 (Caldeira and Wickett 2005). On the other hand, the exposure of resident taxa to lower pH conditions may afford such organisms some degree of evolutionary advantage in future oceans. Indeed, adult *Mytilus edulis*, another mussel species forming dense beds, does not exhibit a strong sensitivity to lowered calcium carbonate saturation state (Ries et al. 2009; Fig. 7b), which could reflect its long history of exposure to the altered chemistry characteristic of bed interstices. The potential for other organisms to adapt genetically to large pH changes has been documented previously (Calosi et al. 2013; reviewed in Hofmann et al. 2014). However, it remains to be seen whether the more modest pH gradients internal to mussel beds are providing a selective pressure influencing adaptive capacity, or whether organisms are simply balancing the added physiological cost with the recognized facilitative benefits of mussel beds with respect to other stressors (e.g., wave forces, high temperatures, and desiccation; Denny 1988; Gaylord 1999; Jurgens and Gaylord 2016, 2018).

Conclusions

Our findings demonstrate the ability of a heterotrophic habitat forming mussel species, *Mytilus californianus*, to alter seawater chemistry inside the beds they create. Importantly, this change operates at the spatial scale experienced by habitat residents. We measured decreases in pH equivalent to those that have occurred in open-ocean environments since preindustrial times (> 0.1 pH). Likewise, we see declines in calcite saturation state that are comparable to reductions expected generally in the sea over the next few decades (> 0.3 Ω_{Ca}). Up to 10% of available oxygen can be depleted within the interstices of submerged *M. californianus* beds. The magnitudes of these shifts depend on flow velocity and biological consumption rates (respiration and calcification), where lower flow and higher rates lead to increased modifications to the chemistry. Through comparisons of these observations to flow speeds measured in the field, we can anticipate that for as much as 98% of the time, seawater within estuarine mussel beds or those occurring subtidally in modestly protected locales may experience reductions of 0.1 pH and 12.1 μmol O_2 kg^{-1} relative to the surrounding seawater. These results indicate that species living within these biogenic habitats may incur trade-offs. On one hand, such habitats provide recruitment substrate, shelter residents from thermal and desiccation stress, and attenuate wave forces. At the same time, there may be costs to living within these beds due to their effects on chemical conditions in their interiors at high tide. Future efforts should explore whether these costs will exacerbate those associated with a changing ocean or whether the chemical stresses active within biogenic habitats will, instead, help prepare resident species for that change.

References

Agostini, S., H. Fujimura, T. Higuchi, I. Yuyama, B. E. Casareto, Y. Suzuki, and Y. Nakano. 2013. The effects of thermal and high-CO_2 stresses on the metabolism and surrounding microenvironment of the coral *Galaxea fascicularis*. C. R. Biol. **336**: 384–391. doi:10.1016/j.crvi.2013.07.003.

Asmus, H., R. M. Asmus, T. C. Prins, N. Dankers, G. Francés, B. Maaß, and K. Reise. 1992. Benthic-pelagic flux rates on mussel beds: Tunnel and tidal flume methodology compared. Helgoländer Meeresunter **46**: 341–361. doi:10.1007/BF02367104.

Barnes, D. J. 1983. Profiling coral reef productivity and calcification using pH and oxygen electrodes. J. Exp. Mar. Biol. Ecol. **66**: 149–161. doi:10.1016/0022-0981(83)90036-9.

Bayne, B. L. 1964. Primary and secondary settlement in *Mytilus-Edulis*-L (Mollusca). J. Anim. Ecol. **33**: 513–523. doi:10.2307/2569.

Bird, R. B., W. E. Stewart, and E. N. Lightfoot. 1960. Transport phenomena. John Wiley & Sons.

Boudreau, B. P., and B. B. Jorgensen [eds.]. 2001. The benthic boundary layer: Transport processes and biogeochemistry. Oxford Univ. Press.

Bresnahan, P. J., T. R. Martz, Y. Takeshita, K. S. Johnson, and M. LaShomb. 2014. Best practices for autonomous measurement of seawater pH with the Honeywell Durafet. Methods Oceanogr. **9**: 44–60. doi:10.1016/j.mio.2014.08.003.

Bruno, J. F., J. J. Stachowicz, and M. D. Bertness. 2003. Inclusion of facilitation into ecological theory. Trends Ecol. Evol. **18**: 119–125. doi:10.1016/S0169-5347(02)00045-9.

Bulleri, F. 2009. Facilitation research in marine systems: State of the art, emerging patterns and insights for future developments. J. Ecol. **97**: 1121–1130. doi:10.1111/j.1365-2745.2009.01567.x.

Burnham, K. P., and D. R. Anderson. 2002. Model selection and multimodel inference: A practical information-theoretic approach, 2nd ed. Springer-Verlag.

Byrne, M. 2011. Impact of ocean warming and ocean acidification on marine invertebrate life history stages: Vulnerabilities and potential for persistence in a changing ocean. Oceanogr. Mar. Biol. An Annu. Rev. **49**: 1–42. doi:10.1016/j.marenvres.2011.10.00.

Byrne, M., and R. Przeslawski. 2013. Multistressor impacts of warming and acidification of the ocean on marine invertebrates' life histories. Integr. Comp. Biol. **53**: 582–596. doi:10.1093/icb/ict049.

Caldeira, K., and M. E. Wickett. 2003. Anthropogenic carbon and ocean pH. Nature **425**: 365–365. doi:10.1038/425365a.

Caldeira, K., and M. E. Wickett. 2005. Ocean model predictions of chemistry changes from carbon dioxide emissions to the atmosphere and ocean. J. Geophys. Res. **110**: C09S04. doi:10.1029/2004JC002671.

Calosi, P., and others. 2013. Adaptation and acclimatization to ocean acidification in marine ectotherms: An in situ transplant experiment with polychaetes at a shallow CO_2 vent system. Philos. Trans. R. Soc. B Biol. Sci. **368**: 1–15.

Carrington, E., G. M. Moeser, S. B. Thompson, L. C. Coutts, and C. A. Craig. 2008. Mussel attachment on rocky shores: The effect of flow on byssus production. Integr. Comp. Biol. **48**: 801–807. doi:10.1093/icb/icn078.

Chan, N. C. S., D. Wangpraseurt, M. Kühl, and S. R. Connolly. 2016. Flow and coral morphology control coral surface pH: Implications for the effects of ocean acidification. Front. Mar. Sci. **3**: 1–11. doi:10.3389/fmars.2016.00010.

Clayton, T. D., and R. H. Byrne. 1993. Spetrophotometric seawater pH measurements: Total hydrogen ion concentration scale calibration of *m*-cresol purple and at-sea results. Deep Sea Res. I **40**: 2115–2129.

Comeau, S., C. E. Cornwall, T. M. Decarlo, E. Krieger, and M. T. Mcculloch. 2018. Similar controls on calcification under ocean acidification across unrelated coral reef taxa. Glob. Chang. Biol. **24**: 4857–4868. doi:10.1111/gcb.14379.

Cornwall, C. E., C. D. Hepburn, C. A. Pilditch, and C. L. Hurd. 2013. Concentration boundary layers around complex assemblages of macroalgae: Implications for the effects of ocean acidification on understory coralline algae. Limnol. Oceanogr. **58**: 121–130. doi:10.4319/lo.2013.58.1.0121.

Dame, R. F., J. D. Spurrier, and R. G. Zingmark. 1992. In-situ metabolism of an oyster reef. J. Exp. Mar. Biol. Ecol. **164**: 147–159.

Dankers, N., R. F. Dame, and K. Kersting. 1989. The oxygen consumption of mussel beds in the Dutch Wadden Sea. Top. Mar. Biol. **53**: 473–476.

Dayton, P. 1972. Toward an understanding of community resilience and the potential effects of enrichment to the benthos at McMurdo Sound, Antarctica. *In* B. Parker [ed.], Proceedings of the colloquium on conservation problems in Antarctica. Allen Press.

Denny, M. W. 1988. Biology and the mechanics of the wave-swept environment. Princeton Univ. Press.

Dixson, D. L., P. L. Munday, and G. P. Jones. 2010. Ocean acidification disrupts the innate ability of fish to detect predator olfactory cues. Ecol. Lett. **13**: 68–75. doi:10.1111/j.1461-0248.2009.01400.x.

Fassbender, A. J., C. L. Sabine, and K. M. Feifel. 2016. Consideration of coastal carbonate chemistry in understanding biological calcification. Geophys. Res. Lett. **43**: 4467–4476. doi:10.1002/2016GL068860.

Frieder, C. A., S. H. Nam, T. R. Martz, and L. A. Levin. 2012. High temporal and spatial variability of dissolved oxygen and pH in a nearshore California kelp forest. Biogeosciences **9**: 3917–3930. doi:10.5194/bg-9-3917-2012.

Gattuso, J.-P., J. Epitalon, and H. Lavigne. 2018. seacarb: Seawater carbonate chemistry.

Gaylord, B. 1999. Detailing agents of physical disturbance: Wave-induced velocities and accelerations on a rocky shore. J. Exp. Mar. Biol. Ecol. **239**: 85–124. doi:10.1016/S0022-0981(99)00031-3.

Gaylord, B., T. M. Hill, E. Sanford, E. A. Lenz, L. A. Jacobs, K. N. Sato, A. D. Russell, and A. Hettinger. 2011. Functional impacts of ocean acidification in an ecologically critical foundation species. J. Exp. Biol. **214**: 2586–2594. doi:10.1242/jeb.055939.

Gaylord, B., and others. 2015. Ocean acidification through the lens of ecological theory. Ecology **96**: 3–15.

Gaylord, B., D. C. Reed, P. T. Raimondi, and L. Washburn. 2006. Macroalgal spore dispersal in coastal environments: Mechanistic insights revealed by theory and experiment. Ecol. Monogr. **76**: 481–502. doi:10.1890/0012-9615(2006)076[0481:MSDICE]2.0.CO;2.

Gazeau, F., J.-P. Gattuso, C. Dawber, A. E. Pronker, F. Peene, J. Peene, C. H. R. Heip, and J. J. Middelburg. 2010. Effect of ocean acidification on the early life stages of the blue mussel *Mytilus edulis*. Biogeosciences **7**: 2051–2060. doi:10.5194/bg-7-2051-2010.

Gazeau, F., and others. 2013. Impacts of ocean acidification on marine shelled molluscs. Mar. Biol. **160**: 2207–2245. doi:10.1007/s00227-013-2219-3.

Green, M. A., G. G. Waldbusser, S. L. Reilly, K. Emerson, and S. O'Donnell. 2009. Death by dissolution: Sediment saturation state as a mortality factor for juvenile bivalves. Limnol. Oceanogr. **54**: 1037–1047. doi:10.4319/lo.2009.54.4.1037.

Green, M. O., J. E. Hewitt, and S. F. Thrush. 1998. Seabed drag coefficient over natural beds of horse mussels (*Atrina zelandica*). J. Mar. Res. **56**: 613–637. doi:10.1357/002224098765213603.

Gutiérrez, J. L., C. G. Jones, D. L. Strayer, and O. O. Iribarne. 2003. Mollusks as ecosystem engineers: The role of shell production engineers in aquatic habitats. Oikos **101**: 79–90.

Hadfield, M. G., and V. Paul. 2001. Natural chemical cues for settlement and metamorphosis of marine-invertebrate larvae. In: McClintock J. and B. Baker [eds.]. Marine Chemical Ecology. CRC Press, Boca Raton, pp 431–462. doi:10.1201/9781420036602.ch13.

Hendriks, I. E., Y. S. Olsen, L. Ramajo, L. Basso, A. Steckbauer, T. S. Moore, J. Howard, and C. M. Duarte. 2014. Photosynthetic activity buffers ocean acidification in seagrass meadows. Biogeosciences **11**: 333–346. doi:10.5194/bg-11-333-2014.

Hofmann, G. E., and others. 2014. Exploring local adaptation and the ocean acidification seascape--studies in the California current large marine ecosystem. Biogeosciences **11**: 1053–1064. doi:10.5194/bg-11-1053-2014.

Hurd, C. L. 2000. Water motion, marine macroalgal physiology, and production. J. Phycol. **36**: 453–472.

Hurd, C. L. 2015. Slow-flow habitats as refugia for coastal calcifiers from ocean acidification. J. Phycol. **51**: 599–605. doi:10.1111/jpy.12307.

Jansen, J. M., H. Hummel, and S. W. Bonga. 2009. The respiratory capacity of marine mussels (*Mytilus galloprovincialis*) in relation to the high temperature threshold. Comp. Biochem. Physiol. Part A **153**: 399–402. doi:10.1016/j.cbpa.2009.03.013.

Jellison, B. M., A. T. Ninokawa, T. M. Hill, E. Sanford, and B. Gaylord. 2016. Ocean acidification alters the response of intertidal snails to a key sea star predator. Proc. R. Soc. B Biol. Sci. **283**: 20160890. doi:10.1098/rspb.2016.0890.

Jokiel, P. L. 2013. Coral reef calcification: Carbonate, bicarbonate and proton flux under conditions of increasing ocean acidification. Proc. R. Soc. B Biol. Sci. **280**: 20130031–20130031. doi:10.1098/rspb.2013.0031.

Jones, C. G., J. H. Lawton, and M. Shachak. 1994. Organisms as ecosystem engineers. Oikos **69**: 373–386. doi:10.2307/3545850.

Jurgens, L. J., and B. Gaylord. 2016. Edge effects reverse facilitation by a widespread foundation species. Sci. Rep. **6**: 1–10. doi:10.1038/srep37573.

Jurgens, L. J., and B. Gaylord. 2018. Physical effects of habitat-forming species override latitudinal trends in temperature. Ecol. Lett. **21**: 190–196. doi:10.1111/ele.12881.

Kanter, R. G. 1979. Biogeographic patterns in mussel community distribution from the Southern California Bight, p. 341–355. *In* The California Islands: Proceedings of a Multidisciplinary Symposium. Santa Barbara Museum of Natural History.

Kelley, D., and C. Richards. 2018. oce: Analysis of Oceanographic data.

Khripounoff, A., J. C. Caprais, C. Decker, J. Le Bruchec, P. Noel, and B. Husson. 2017. Respiration of bivalves from three different deep-sea areas: Cold seeps, hydrothermal vents and organic carbon-rich sediments. Deep Sea Res. Part II Top. Stud. Oceanogr. **142**: 233–243. doi:10.1016/j.dsr2.2016.05.023.

Kinsey, D. W. 1985. Metabolism, calcification and carbon production. Proc. Fifth Int. Coral Reef Congr **4**: 505–526.

Koweek, D. A., and others. 2017. A year in the life of a central California kelp forest: Physical and biological insights into biogeochemical variability. Biogeosciences **14**: 31–44. doi:10.5194/bg-14-31-2017.

Koweek, D. A., and others. 2018. Expected limits on the ocean acidification buffering potential of a temperate seagrass meadow. Ecol. Appl. Ther. **28**: 1694–1714. doi:10.1002/eap.1771.

Kroeker, K. J., R. L. Kordas, R. N. Crim, and G. G. Singh. 2010. Meta-analysis reveals negative yet variable effects of ocean acidification on marine organisms. Ecol. Lett. **13**: 1419–1434. doi:10.1111/j.1461-0248.2010.01518.x.

Kurihara, H. 2008. Effects of CO_2-driven ocean acidification on the early developmental stages of invertebrates. Mar. Ecol. Prog. Ser. **373**: 275–284. doi:10.3354/meps07802.

Kwiatkowski, L., and others. 2016. Nighttime dissolution in a temperate coastal ocean ecosystem increases under acidification. Sci. Rep. **6**: 1–9. doi:10.1038/srep22984.

Lafferty, K. D., and T. H. Suchanek. 2016. Revisiting Paine's 1966 sea star removal experiment, the most-cited empirical article in the American Naturalist. Am. Nat. **188**: 365–378. doi:10.1086/688045.

Lantz, C. A., M. J. Atkinson, C. W. Winn, and S. E. Kahng. 2014. Dissolved inorganic carbon and total alkalinity of a Hawaiian fringing reef: Chemical techniques for monitoring the effects of ocean acidification on coral reefs. Coral Reefs **33**: 105–115. doi:10.1007/s00338-013-1082-5.

Levin, L. A., and others. 2009. Effects of natural and human-induced hypoxia on coastal benthos. Biogeosciences **6**: 2063–2098. doi:10.5194/bg-6-2063-2009.

Lueker, T. J., A. G. Dickson, and C. D. Keeling. 2000. Ocean pCO_2 calculated from dissolved inorganic carbon, alkalinity, and equations for K_1 and K_2: Validation based on laboratory measurements of CO_2 in gas and seawater at equilibrium. Mar. Chem. **70**: 105–119. doi:10.1016/S0304-4203(00)00022-0.

Malone, P. G., and J. R. Dodd. 1967. Temperature and salinity effects on calcification rate in *Mytilus edulis* and its paleoecological implications. Limnol. Oceanogr. **12**: 432–436. doi:10.4319/lo.1967.12.3.0432.

Martz, T. R., J. G. Connery, and K. S. Johnson. 2010. Testing the Honeywell Durafet® for seawater pH applications. Limnol. Oceanogr.: Methods **8**: 172–184. doi:10.4319/lom.2010.8.172.

McGillis, W. R., C. Langdon, B. Loose, K. K. Yates, and J. Corredor. 2011. Productivity of a coral reef using boundary layer and enclosure methods. Geophys. Res. Lett. **38**: 1–5. doi:10.1029/2010GL046179.

Munday, P. L., D. L. Dixson, M. I. McCormick, M. Meekan, M. C. O. Ferrari, and D. P. Chivers. 2010. Replenishment of fish populations is threatened by ocean acidification. Proc. Natl. Acad. Sci. **107**: 12930–12934. doi:10.1073/pnas.1004519107.

Nixon, S. W., C. A. Oviatt, C. Rogers, and K. Taylor. 1971. Mass and metabolism of a mussel bed. Oecologia **8**: 21–30. doi:10.1007/BF00345624.

Page, H. N., and others. 2016. Differential modification of seawater carbonate chemistry by major coral reef benthic communities. Coral Reefs **35**: 1311–1325. doi:10.1007/s00338-016-1490-4.

Ries, J. B., A. L. Cohen, and D. C. McCorkle. 2009. Marine calcifiers exhibit mixed responses to CO_2-induced ocean acidification. Geology **37**: 1131–1134. doi:10.1130/G30210A.1.

Ries, J. B., M. N. Ghazaleh, B. Connolly, I. Westfield, and K. D. Castillo. 2016. Impacts of seawater saturation state (ΩA = 0.4–4.6) and temperature (10, 25°C) on the dissolution kinetics of whole-shell biogenic carbonates. Geochim. Cosmochim. Acta **192**: 318–337. doi:10.1016/j.gca.2016.07.001.

Robinson, C. 2019. Microbial respiration, the engine of ocean deoxygenation. Front. Mar. Sci. **5**: 1–13. doi:10.3389/fmars.2018.00533.

Ruginis, T., M. Zilius, I. Vybernaite-Lubiene, J. Petkuviene, and M. Bartoli. 2017. Seasonal effect of zebra mussel colonies on benthic processes in the temperate mesotrophic Plateliai Lake, Lithuania. Hydrobiologia **802**: 23–38. doi:10.1007/s10750-017-3237-9.

Saarman, N. P., and G. H. Pogson. 2015. Introgression between invasive and native blue mussels (genus Mytilus) in the central California hybrid zone. Mol. Ecol. **24**: 4723–4738. doi:10.1111/mec.13340.

Shashar, N., Y. Cohen, and Y. Loya. 1993. Extreme diel fluctuations of oxygen in diffusive boundary layers surrounding stony corals. Biol. Bull. **185**: 455–461.

Small, A. M., W. H. Adey, and D. Spoon. 1998. Are current estimates of coral reef biodiversity too low? The view through the window of a microcosm. Atoll Res. Bull. **458**: 1–20. doi:10.5479/si.00775630.458.1.

Soetaert, K., T. Petzoldt, and F. Meysman. 2018. marelac: Tools for aquatic sciences.

Stickle, W. B., and Sabourin. 1979. Effects of salinity on the respiration and heart rate of the common mussel, *Mytilus edulis* L., and the black chiton, *Katherina Tunicata* (Wood). J. Exp. Mar. Biol. Ecol. **41**: 257–268.

Stocking, J. B., J. P. Rippe, and M. A. Reidenbach. 2016. Structure and dynamics of turbulent boundary layer flow over healthy and algae-covered corals. Coral Reefs **35**: 1047–1059. doi:10.1007/s00338-016-1446-8.

Takeshita, Y., T. Cyronak, T. R. Martz, T. Kindeberg, and A. J. Andersson. 2018. Coral reef carbonate chemistry variability at different functional scales. Front. Mar. Sci. **5**: 1–5. doi:10.3389/fmars.2018.00175.

Takeshita, Y., W. Mcgillis, E. M. Briggs, A. L. Carter, E. M. Donham, T. R. Martz, N. N. Price, and J. E. Smith. 2016. Assessment of net community production and calcification of a coral reef using a boundary layer approach. J. Geophys. Res. Ocean. **121**: 5655–5671. doi:10.1002/2016JC011886.

Thomsen, J., K. Haynert, K. M. Wegner, and F. Melzner. 2015. Impact of seawater carbonate chemistry on the calcification of marine bivalves. Biogeosciences **12**: 4209–4220. doi:10.5194/bg-12-4209-2015.

Uppstrom, L.R. 1974. The boron/chlorinity ratio of the deep-sea water from the Pacific Ocean. Deep-Sea Research **21**: 161–162. doi:10.1016/0011-7471(74)90074-6.

Vaquer-Sunyer, R., and C. M. Duarte. 2008. Thresholds of hypoxia for marine biodiversity. Proc. Natl. Acad. Sci. **105**: 15452–15457. doi:10.1073/pnas.0803833105.

Wahl, M., S. Schneider Covachã, V. Saderne, C. Hiebenthal, J. D. Müller, C. Pansch, and Y. Sawall. 2017. Macroalgae may mitigate ocean acidification effects on mussel calcification by increasing pH and its fluctuations. Limnol. Oceanogr. **63**: 3–21. doi:10.1002/lno.10608.

Waldbusser, G. G., and others. 2015. Ocean acidification has multiple modes of action on bivalve larvae. PLoS One **10**: 10. doi:10.1371/journal.pone.0128376.

Whedon, W. F., and H. Z. Sommer. 1937. Respiratory exchange of *Mytilus californianus*. J. Comp. Physiol. **25**: 523–528.

Witman, J. D., and T. H. Suchanek. 1984. Mussels in flow: Drag and dislodgement by epizoans. Mar. Ecol. Prog. Ser. **16**: 259–268. doi:10.3354/meps016259.

Zeebe, R. E., and D. A. Wolf-Gladrow. 2001. CO_2 in seawater: Equilibrium, kinetics, isotopes. Elsevier.

Acknowledgments

This work was supported by National Science Foundation (NSF) OCE-1636191 and A.N. was additionally supported by an NSF Graduate Research Fellowship. Comments from J. Leichter and two anonymous reviewers improved the manuscript. The authors are also grateful to K. Caldeira for loaning several sensors, and thank G. Susner and K. Hewett for helpful discussions regarding sensors and data analysis, and B. O'Donnell and W. Calhoun for assistance with mussel collection.

Conflict of Interest

None declared

Submitted 01 December 2018
Revised 26 March 2019
Accepted 24 June 2019

Associate editor: James Leichter